BJP British Journal of Pharmacology

DOI:10.1111/j.1476-5381.2012.02004.x
www.brjpharmacol.org

RESEARCH PAPER

Mechanism and molecular basis for the sodium channel subtype specificity of μ-conopeptide CnIIIC

René Markgraf[1]*, Enrico Leipold[1]*, Jana Schirmeyer[1], Marianne Paolini-Bertrand[2], Oliver Hartley[2] and Stefan H Heinemann[1]

[1]*Center for Molecular Biomedicine, Department of Biophysics, Friedrich Schiller University of Jena & Jena University Hospital, Jena, Germany, and* [2]*Department of Structural Biology and Bioinformatics, University of Geneva, Geneva, Switzerland*

Correspondence
Professor and Dr. Stefan H Heinemann, Center for Molecular Biomedicine, Department of Biophysics, Friedrich Schiller University of Jena & Jena University Hospital, Hans-Knoell-Str. 2, Jena D-07745, Germany. E-mail: stefan.h.heinemann@uni-jena.de

*These authors contributed equally to this work as first author.

Keywords
sodium channel; muscle relaxant; analgesia; conotoxin; patch-clamp

Received
8 November 2011
Revised
4 April 2012
Accepted
17 April 2012

BACKGROUND AND PURPOSE

Voltage-gated sodium channels (Na_V channels) are key players in the generation and propagation of action potentials, and selective blockade of these channels is a promising strategy for clinically useful suppression of electrical activity. The conotoxin μ-CnIIIC from the cone snail *Conus consors* exhibits myorelaxing activity in rodents through specific blockade of skeletal muscle ($Na_V1.4$) Na_V channels.

EXPERIMENTAL APPROACH

We investigated the activity of μ-CnIIIC on human Na_V channels and characterized its inhibitory mechanism, as well as the molecular basis, for its channel specificity.

KEY RESULTS

Similar to rat paralogs, human $Na_V1.4$ and $Na_V1.2$ were potently blocked by μ-CnIIIC, the sensitivity of $Na_V1.7$ was intermediate, and $Na_V1.5$ and $Na_V1.8$ were insensitive. Half-channel chimeras revealed that determinants for the insensitivity of $Na_V1.8$ must reside in both the first and second halves of the channel, while those for $Na_V1.5$ are restricted to domains I and II. Furthermore, domain I pore loop affected the total block and therefore harbours the major determinants for the subtype specificity. Domain II pore loop only affected the kinetics of toxin binding and dissociation. Blockade by μ-CnIIIC of $Na_V1.4$ was virtually irreversible but left a residual current of about 5%, reflecting a 'leaky' block; therefore, Na^+ ions still passed through μ-CnIIIC-occupied $Na_V1.4$ to some extent. TTX was excluded from this binding site but was trapped inside the pore by μ-CnIIIC.

CONCLUSION AND IMPLICATIONS

Of clinical significance, μ-CnIIIC is a potent and persistent blocker of human skeletal muscle $Na_V1.4$ that does not affect activity of cardiac $Na_V1.5$.

Abbreviations

DTNP, 2,2′-dithiobis(5-nitropyridine); Na_V channel, voltage-gated sodium channel; TTX, tetrodotoxin

Introduction

Voltage-gated sodium channels (Na_V channels) are essential for rapid electrical signalling in neuronal and muscle cells. This important role is manifested by an array of muscular and neuronal diseases associated with either Na_V channel inhibition or hyperactivity (e.g. George, 2005; Andavan and Lemmens-Gruber, 2011). Numerous drugs bind to Na_V

channels and are used to interfere with neuronal signalling, mainly to dampen electrical firing to achieve analgesia (e.g. Priest, 2009; Zuliani *et al.*, 2010). However, since in humans there are nine genes coding for prototypical Na_V channels, not all of which are implicated in pain signalling (Goldin, 2002; Wood *et al.*, 2004); safe and effective pharmacological interference with Na_V channels requires subtype-specific drugs. For example, Na_V channel inhibitors used as analgesics should not affect cardiac Na_V channels ($Na_V1.5$) or those expressed in the CNS ($Na_V1.1$, $Na_V1.2$). Hence, there is a significant demand for new drugs with high specificity for Na_V channel subtypes that are strongly expressed in the peripheral nervous system, for example, $Na_V1.3$, $Na_V1.6$ or $Na_V1.7$. The strong structural conservation across the Na_V channel subtypes makes this a difficult challenge for standard medicinal chemistry approaches.

Peptides from marine cone snails, referred to as conotoxins, may provide specific Na_V channel inhibitors. Among them, μ-conotoxins are particularly promising candidates because they block the pore of Na_V channels from the extracellular side. With a size of 16–26 amino acid residues and three disulfide bridges, μ-conotoxins are large enough to make contact with all four domains of a Na_V channel α-subunit (Dudley *et al.*, 2000; Li *et al.*, 2001; Choudhary *et al.*, 2003). Therefore, in contrast to low molecular weight compounds, μ-conotoxins have the potential to be tailored so that they 'fit' perfectly to one specific Na_V subtype only. A detailed understanding of how μ-conotoxins interact with and block Na_V channel subtypes is therefore likely to be the key to future drug development (for review, see Norton, 2010).

One candidate holding such promise is μ-CnIIIC, a 22-residue conopeptide from *Conus consors*, which displays long-lasting myorelaxing effects in rodents (Favreau *et al.*, 2012). This activity is due to its ability to potently block rat skeletal muscle $Na_V1.4$ and rat brain $Na_V1.2$ channels. μ-CnIIIC does not block cardiac mouse $Na_V1.5$ channels and rat dorsal root ganglia $Na_V1.8$ channels and shows intermediate inhibitory activity on neuronal mouse $Na_V1.6$ and $Na_V1.7$ channels. In order to further the development of μ-CnIIIC as a highly selective Na_V-targeting drug or lead structure, we set out to determine whether μ-CnIIIC shows a similar specificity pattern for human Na_V channel subtypes. In addition, we used Na_V channel chimeras to elucidate the location of molecular determinants for sensitivity and insensitivity to μ-CnIIIC and to investigate the mechanism by which it blocks the target channels.

Methods

Production of μ-CnIIIC

μ-CnIIIC, with the sequence of ZGCCNGPKGCSSKWCR DHARCC-NH_2 (Z = pyroglutamate), was synthesized and folded as described in Favreau *et al.* (2012).

Generation of channel mutants

Wild-type Na_V channels used in this study were the rat (r) isoforms of $Na_V1.4$ (SCN4A, P15390) and $Na_V1.8$ (SCN10A, Q62968) and the human (h) isoforms of $Na_V1.2$ (SCN2A, Q99250), $Na_V1.4$ (SCN4A, P35499), $Na_V1.5$ (SCN5A, Q14524), $Na_V1.7$ (SCN9A, Q15858) and $Na_V1.8$ (SCN10A, Q9Y5Y9.2). Accession numbers refer to the UniProt database, and nomenclature is according to Alexander *et al.* (2011).

Construction of domain chimeras between $rNa_V1.4$ and $hNa_V1.5$ was as described previously (Leipold *et al.*, 2011); we either introduced single domains of $hNa_V1.5$ into the background of $rNa_V1.4$ yielding 5444, 4544, 4454 and 4445 or replaced the first or second half of the channel protein for constructs 5544 and 4455. In addition, pore loops of $hNa_V1.5$ were inserted into the background of $rNa_V1.4$: domain I, from I239 to A443, termed Ip5; domain II, from G692 to V766, termed IIp5 (numbers refer to $rNa_V1.4$; see supporting information Figure S2). The combination is termed Ip5-IIp5. Similarly, pore loops of $Na_V1.7$ were introduced into $Na_V1.4$ (Ip7, IIp7 and Ip7-IIp7). Further site-directed mutagenesis was performed following PCR strategies. Half-channel chimeras between $rNa_V1.4$ and $rNa_V1.8$ were constructed according to an equivalent strategy yielding 4488 and 8844; the boundary was between residues A1040 and L1041 in $rNa_V1.4$ and A1169 and L1170 in $rNa_V1.8$ respectively. Constructs based on $Na_V1.8$ had to be expressed in Neuro-2A cells, and current recording was done in the presence of 1 μM TTX to completely block endogenous Na_V channels. Chimera 4488 was thus mutated in the pore loop of domain I (Y401S) to render this channel insensitive to TTX and, hence, to make it accessible for functional assays in Neuro-2A cells; this construct was termed 4*488. Mutant $rNa_V1.4$-Y401S served as a control.

All mutant channel constructs were verified by DNA sequencing. Plasmid DNA was isolated from *E. coli* using the PureYield plasmid purification kit (Promega GmbH, Mannheim, Germany).

Cell culture and transfection

HEK 293 cells (Centre for Applied Microbiology and Research, Porton Down, Salisbury, UK) were maintained in 45% Dulbecco's modified Eagles medium and 45% Ham's F12 Medium, supplemented with 10% fetal calf serum in a 5% CO_2 incubator at 37°C. HEK 293 cells were trypsinized, diluted with culture medium and grown in 35 mm dishes. When grown to 30–50% confluence, the cells were transfected with a 5:1 ratio of the Na_V channel expression plasmids and a vector encoding the CD8 antigen (Jurman *et al.*, 1994) using the Rotifect transfection kit (Roth, Karlsruhe, Germany). Dynabeads (Deutsche Dynal GmbH, Hamburg, Germany) were used for visual identification of individual transfected cells. For expression of $Na_V1.8$ channels, Neuro-2A cells [German Collection of Microorganisms and Cell Cultures (DSMZ), Braunschweig, Germany] were used. Endogenous sodium channels of Neuro-2A cells were blocked with 1 μM TTX.

Electrophysiological recordings

Sodium current was measured by applying the whole-cell configuration of the patch-clamp method to HEK 293 and Neuro-2A (for $Na_V1.8$) cells 24–48 h after transfection as described previously (Chen *et al.*, 2000; Schirmeyer *et al.*, 2010). Patch pipettes were fabricated from Kimax borosilicate glass of about 1–2 MΩ resistance. EPC-9 and EPC-10 patch clamp amplifiers operated by PatchMaster software (HEKA Elektronik, Lambrecht, Germany) were used. Series resistance was corrected electronically up to 85%; recording configurations with series resistance greater than 5 MΩ were discarded.

The patch pipettes contained (in mM): 35 NaCl, 105 CsF, 10 EGTA, 10 HEPES (pH 7.4 with CsOH). The bath solution contained (in mM): 150 NaCl, 2 KCl, 1.5 $CaCl_2$, 1 $MgCl_2$, 10 HEPES (pH 7.4 with NaOH). μ-CnIIIC was diluted in bath solution containing 2 mg·mL^{-1} BSA and stored at –20°C until use. The toxin was applied locally with a glass pipette as described previously (Chen *et al.*, 2000). Rapid inactivation of mutant rNa$_V$1.4-M1305C was removed by extracellular application of 100 μM 2,2′-dithiobis(5-nitropyridine) (DTNP). All experiments were performed at 20 ± 1°C.

The onset of toxin-induced current block was measured with repetitive pulses to –20 mV every 5 s. Peak currents were plotted as a function of time and fitted with a single-exponential function to estimate the time constant of block, τ, and the steady state current remaining after μ-CnIIIC equilibration (I_{rem}). The concentration-dependence of current block was analysed with a Hill equation; the Hill coefficient, n_H (h in the equation) was set to 1 assuming a first-order reaction of toxin binding:

$$\frac{I_{rem}}{I_{ctrl}} = r_\infty + \frac{1 - r_\infty}{\left(1 + \frac{[\mu - CnIIIC]}{IC_{50}}\right)^h} \quad (1)$$

IC_{50} is the concentration where toxin-induced current block becomes half-maximal and r_∞ the remaining current fraction at limiting toxin concentration. The error of IC_{50} was obtained from the data fit using IgorPro software (WaveMetrics, Lake Oswego, OR, USA). The apparent on-rate k_{on} and off-rate k_{off} of current block were estimated by analysing the inverse of the time constant of current block, τ_{on}, as a function of μ-CnIIIC concentration:

$$\frac{1}{\tau_{on}} = [\mu - CnIIIC] \cdot k_{on} + k_{off} \quad (2)$$

The off-rate, k_{off}, was further constrained by the inverse of the time constant of current recovery measured upon toxin removal, τ_{off}.

Non-stationary noise analysis was performed as described earlier (Starkus *et al.*, 2003; Heinemann and Leipold, 2011). A train off >200 10 ms test depolarizations to various voltages was applied in the absence and presence of 100 μM μ-CnIIIC. The leak-corrected mean current responses and the corresponding variances were calculated using PulseTools software (HEKA Elektronik). Variance was analysed as a function of mean current assuming a binomial distribution of channel states (Sigworth, 1977):

$$\sigma^2 = \sigma_0^2 + \left(i \cdot I + \frac{I^2}{N_{ch}}\right) \quad (3)$$

Where σ^2 is the variance and I is the macroscopic mean current response of all individual test depolarizations. N_{ch} defines the number of channels underlying the macroscopic current, and i is an estimate for the single-channel current. The maximal open probability $P_{o,max}$ was estimated from the variance analysis according to:

$$P_{o,max} = \frac{I_{max}}{i \cdot N_{ch}} \quad (4)$$

Data analysis and statistics

Electrophysiological data were analysed with FitMaster (HEKA Elektronik) and IgorPro (WaveMetrics) software. Data are presented as mean ± SEM with n = number of independent measurements. Significance for the difference between two data groups was tested with a Student's two-sided t-test; the resulting P-values are indicated.

Results

μ-CnIIIC blocks human Na$_V$1.4 channels virtually irreversibly

Rat skeletal muscle Na$_V$1.4 channels are potently blocked by μ-CnIIIC, while mouse cardiac Na$_V$1.5 and rat TTX-resistant Na$_V$1.8 are insensitive (Favreau *et al.*, 2012). We set out to determine whether this clear channel discrimination seen in rodents is also valid for the human paralogs. As shown in Figure 1A and B, hNa$_V$1.4 channels, heterologously expressed in HEK 293 cells, were almost completely blocked by 1 μM μ-CnIIIC. The remaining current of about 5% did not show any obvious alterations in kinetics (Figure 1A). The onset of block, described with a single exponential function (Figure 1B), proceeded with a time constant τ_{on} of about 250 s and even after extensive washing with control saline the current did not recover. Measurements of current block at various μ-CnIIIC concentrations and simultaneous description of the steady-state block and its kinetics according to a first-order reaction (Figure 1C) revealed an apparent IC_{50} value of 4.95 ± 0.50 nM, an on-rate (k_{on}) of 4.1 ± 0.5 10^3 M^{-1}·s^{-1}, a practically vanishing off-rate (k_{off} = 2.0 ± 0.3 10^5 s^{-1}) and a remaining current component at saturating toxin concentration (r_∞) of 4.95 ± 0.12%. These results are very similar to those obtained for rat Na$_V$1.4 (IC_{50} = 1.3 ± 0.4 nM; k_{on} = 3.6 ± 0.7 10^3 M^{-1}·s^{-1}; k_{off} = 4.6 ± 0.7 10^6 s^{-1}; r_∞ = 5.01 ± 0.23%). Hence, importantly, μ-CnIIIC would be expected to inhibit human skeletal muscle Na$_V$ channels in a clinical setting. This block was very slow (based on the determined k_{on}, the time constant for the onset of μ-CnIIIC effect at the IC_{50} was estimated to about 13 h) and extremely long-lasting. Furthermore, the block even persisted when cells were washed with buffered salines covering pH values in the range of 6.5–8.0 (supporting information Figure S1).

Similar experiments were performed for human brain Na$_V$1.2 and human peripheral nerve Na$_V$1.7 (Figure 1D); while Na$_V$1.2 was effectively blocked by 1 μM μ-CnIIIC (I_{rem} = 14.7 ± 5.3%, n = 4), the sensitivity of Na$_V$1.7 was significantly less (I_{rem} = 35.1 ± 4.6%, n = 7, P = 0.02).

Similar to their rodent counterparts, human cardiac Na$_V$1.5 and TTX-resistant Na$_V$1.8 channels were only marginally affected by 10 μM μ-CnIIIC (Figure 1D).

Molecular determinants of channel specificity

Because of the similarity of human and rodent Na$_V$ channels with respect to block by μ-CnIIIC, it appeared justified to search for channel-based molecular determinants responsible for this subtype specificity using chimeras between rNa$_V$1.4 and hNa$_V$1.5 (Leipold *et al.*, 2011) as well as between rNa$_V$1.4 and rNa$_V$1.8 (see Methods). Based on previous studies that identified important interaction sites for μ-conotoxins in the

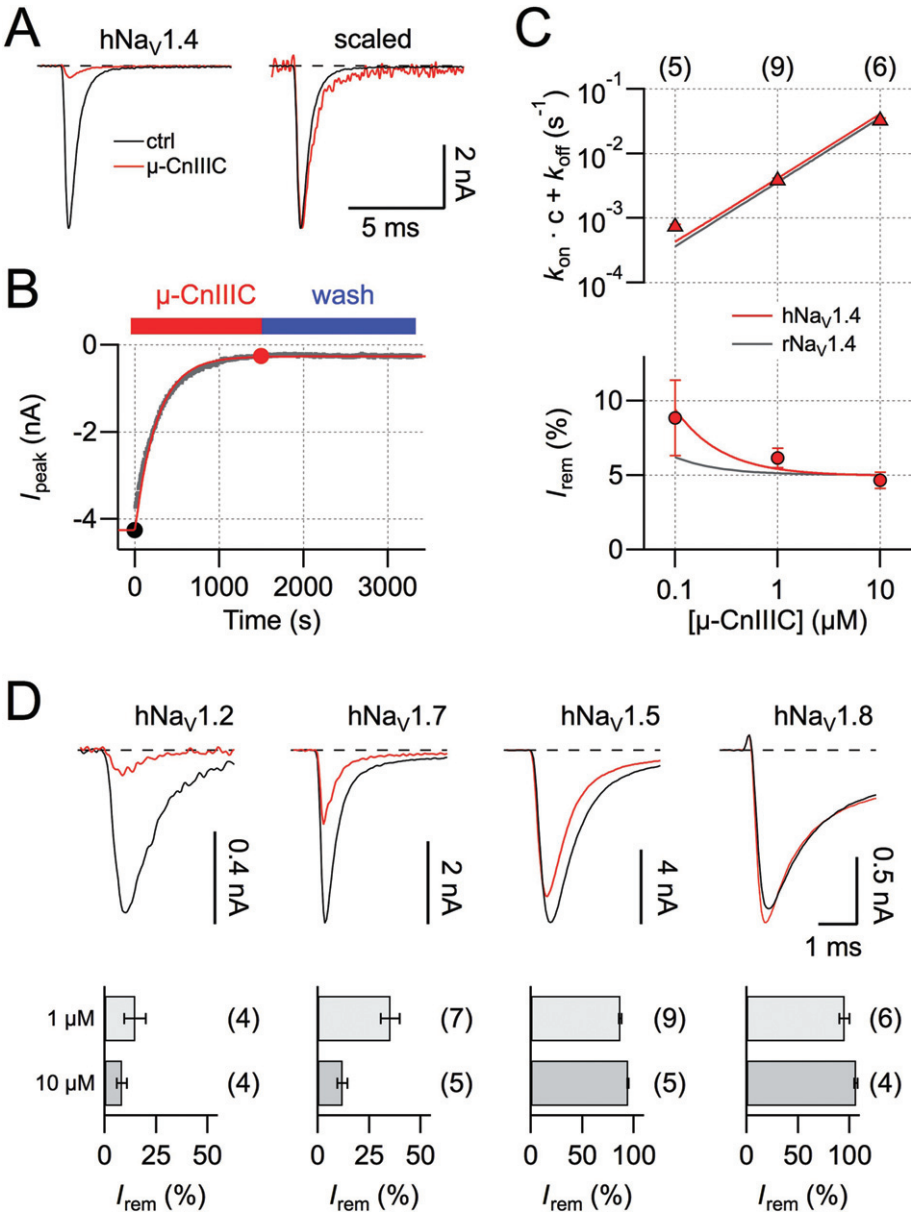

Figure 1

μ-CnIIIC blocks human skeletal muscle $Na_V1.4$ channels. (A) Superposition of current traces recorded at −20 mV before (ctrl) and after application of 1 μM μ-CnIIIC (red). In the panel on the right, the red trace is scaled to match control peak currents, illustrating that the current remaining after μ-CnIIIC application does not exhibit changes in kinetics. (B) Time course of peak current reduction upon application of 1 μM μ-CnIIIC followed by wash. The continuous curve is a single-exponential data fit. Solid symbols indicate data points referring to the traces shown in (A). (C) Inverse of the mean time constant of onset of current block (top) and extrapolated remaining steady-state current (bottom) for three toxin concentrations. Red lines are global fits according to equations 1–2 for human $Na_V1.4$; grey lines are the corresponding fit results for rat $Na_V1.4$. (D) Superposition of current traces for $hNa_V1.2$, $hNa_V1.7$ and $hNa_V1.5$ at −20 mV, as well as $hNa_V1.8$ at 10 mV before (black) and after application of 1 μM μ-CnIIIC (red). The bar graphs show the remaining current after toxin application at the indicated concentrations. The *n* values in (C) and (D) are shown in parentheses.

pore loops of domains I and II (Dudley *et al.*, 1995; 2000; Chahine *et al.*, 1998; Li *et al.*, 2001; Cummins *et al.*, 2002; Leipold *et al.*, 2011), we first assayed channel chimeras in which only one half of the channel protein was replaced, that is, 4455/5544 and 4*488/8844 (each numeral indicates the origin of the respective subunit, see Figure 2A). As shown in Figure 2, all four chimeras gave rise to functional channels. However, the effect of 1 μM μ-CnIIIC differed across the panel of chimeras; while chimera 4455 showed μ-CnIIIC sensitivity comparable to wild-type $Na_V1.4$, chimera 5544 was as insensitive as $Na_V1.5$ (Figure 2B and C). Both chimeras based on $Na_V1.8$ were insensitive to 10 μM μ-CnIIIC (Figure 2D and E), indicating that in $Na_V1.8$ channels, even domains III and IV contain structural elements that prohibit channel block by

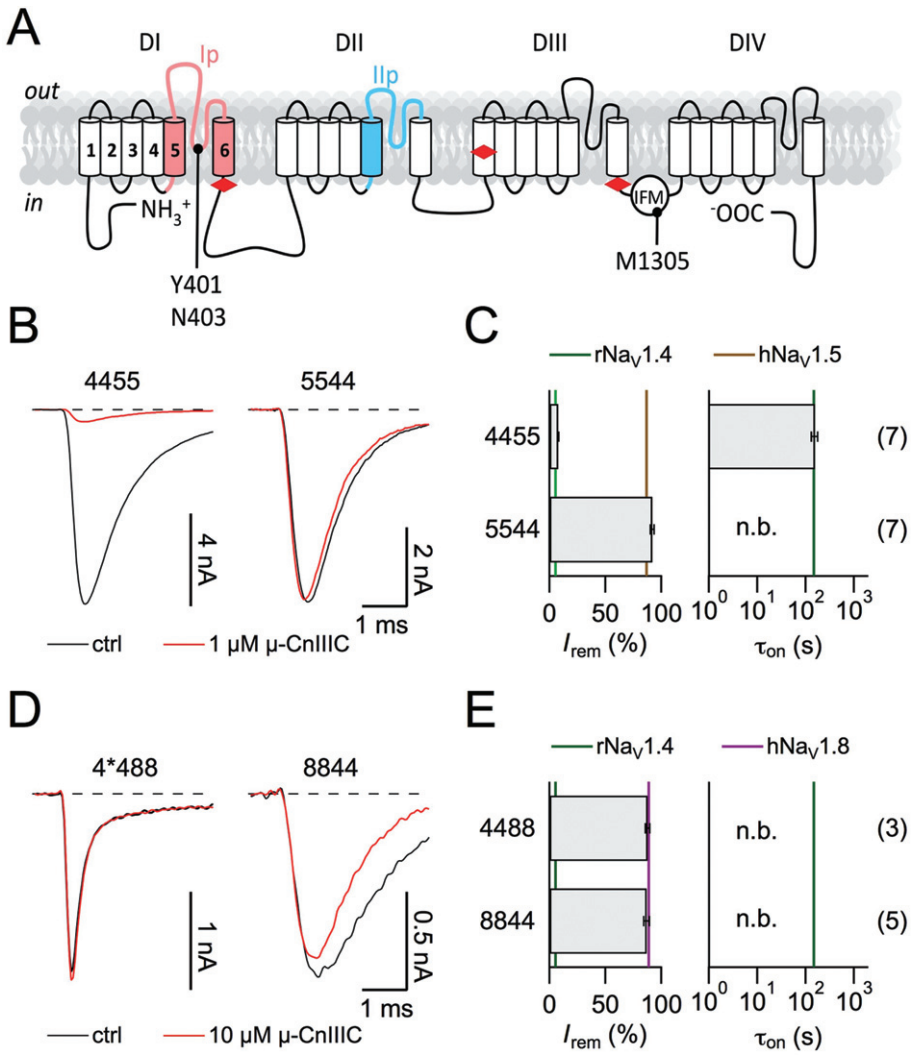

Figure 2

Half-channel chimeras between rNa$_V$1.4 and hNa$_V$1.5/rNa$_V$1.8. (A) Topological cartoon of a Na$_V$ α-subunit with four homologous domains (DI–DIV). Boundaries used for the construction of domain chimeras (red diamonds) and pore loop chimeras are indicated. Residue numbers refer to rNa$_V$1.4. (B, D) Superposition of current traces at –20 mV before (black) and after application of 1 µM µ-CnIIIC (red) for chimeras 4455 and 5544 in HEK 293 cells (B), as well as traces at 10 mV for 4*488 and 8844 in Neuro-2A cells with 10 µM µ-CnIIIC (D). (C, E) Mean remaining current (left) and apparent time constant of onset of block for the indicated chimeras. Vertical lines indicate the mean values of the respective wild-type channels. 'n.b.' refers to a situation where no onset was measured because channels were not blocked. The *n* values are shown in parentheses. Note that chimera 4*488 carries the additional mutation Y401S in order to make this construct resistant to TTX. In the background of rNa$_V$1.4, this mutation does not strongly alter the ability of 1 µM µ-CnIIIC to block the channel (89.5 ± 0.4% block for Y401S, $n = 6$).

this µ-conotoxin, and hence, identification of subtype-specific interaction sites would involve detailed study of the entire channel protein. We decided to focus on further Na$_V$1.4/Na$_V$1.5 chimeras in order to elucidate which structural differences in the first two domains are responsible for the insensitivity of Na$_V$1.5 channels.

We initially focused on the first channel half by comparing chimeras 5444 and 4544 (Figure 3). While incorporation of domain I from Na$_V$1.5 strongly reduced the effect of 1 µM µ-CnIIIC (I_{rem} = 51.9 ± 3.8%, n = 7), incorporation of domain II affected µ-CnIIIC's action to a lesser extent (I_{rem} = 8.5 ± 2.0%, n = 7), indicating that the major discriminating structural component must reside in domain I. Structures present in Na$_V$1.5 not only affect the amount of channel blockade, but also its kinetics. For chimera 5444, the onset of block was about four times faster than for wild-type Na$_V$1.4 channels (τ_{on} = 76.3 ± 5.4 s), and for chimera 4544, it was 20 times faster (τ_{on} = 11.6 ± 1.1 s). Hence, the structures from Na$_V$1.5, while rendering the chimeric channel insensitive to µ-CnIIIC, actually increase the on-rate of the channel–ligand interaction.

Insertion of just the pore loop from Na$_V$1.5 domain I (see Figure 2A) into Na$_V$1.4 (termed Ip5) resulted in a toxin sensitivity profile indistinguishable from that of 5444, the chimera containing the whole Na$_V$1.5 domain I (I_{rem} = 42.5 ± 1.9%, τ_{on} = 91.1 ± 13.6 s, n = 6; Figure 3A). For a multiple sequence

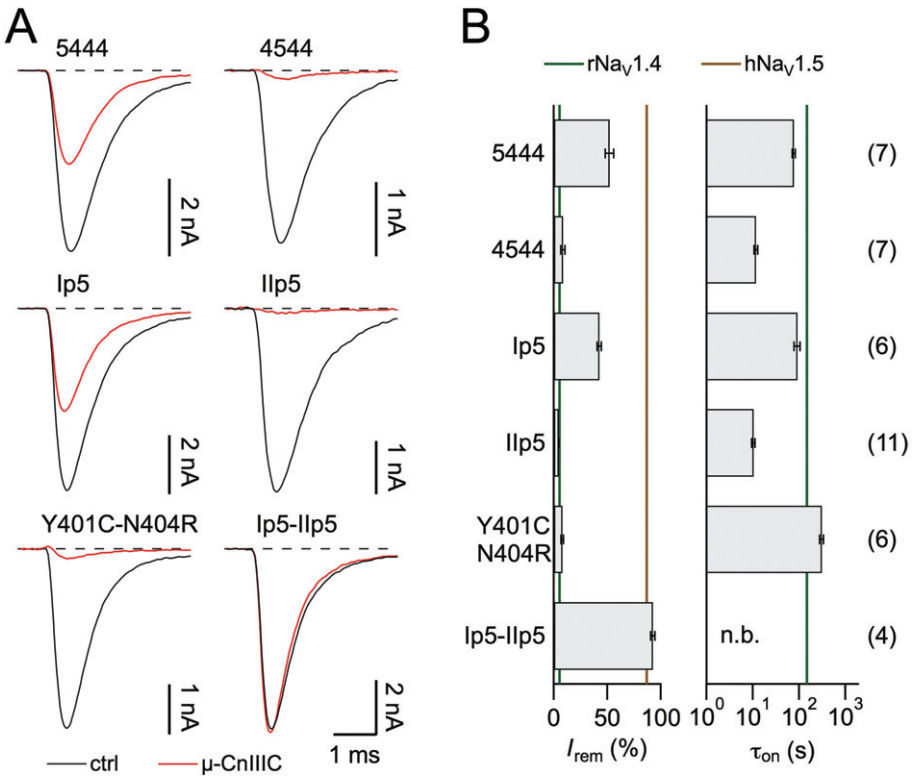

Figure 3

Chimeras between rNa$_V$1.4 and hNa$_V$1.5. (A) Superposition of current traces at –20 mV before (black) and after application of 1 μM μ-CnIIIC (red) for the indicated chimeras and the TTX-site mutant rNa$_V$1.4-Y401C-N404R. (B) Mean remaining current (left) and apparent time constant of onset of block (right) for the indicated chimeras and mutants. Vertical lines indicate mean values for the respective wild-type channels. 'n.b.' refers to a situation where no onset was measured because channels were not blocked. The *n* values are shown in parentheses.

alignment of pore loops from domains I and II see supporting information Figure S2. Similarly, insertion of just the pore loop from Na$_V$1.5 domain II (IIp5) into Na$_V$1.4 resulted in a toxin sensitivity profile resembling that of chimera 4544, the chimera containing the whole Na$_V$1.5 domain II (I_{rem} = 4.5 ± 0.3%, τ_{on} = 10.3 ± 0.9 s, n = 11). The combination of both pore loops (Ip5-IIp5) from Na$_V$1.5 in Na$_V$1.4 reproduced the μ-CnIIIC sensitivity profile of Na$_V$1.5. We can thus conclude that the pore loops of domains I and II, which are sufficient to confer the μ-CnIIIC-related properties from Na$_V$1.5 to Na$_V$1.4, contain the molecular determinants for μ-CnIIIC selectivity. The pore loop of domain I appears to predominantly affect the extent of channel blockade, while the domain II pore loop has a strong impact on the on-rate of toxin binding.

In the inner pore region of domain I, there are two important structural differences between Na$_V$1.4 and Na$_V$1.5 channels: residue Y401 in Na$_V$1.4 permits TTX binding, while the homologous cysteine in Na$_V$1.5 reduces TTX sensitivity (Backx *et al.*, 1992). The positively charged arginine, located in three residues of the C-terminal in Na$_V$1.5, makes the channels more resistant to extracellular divalent cations as compared to Na$_V$1.4 with an asparagine at the homologous position (Heinemann *et al.*, 1992). In addition, it was shown that this site affects channel block by μ-SIIIA from *Conus striatus* (Leipold *et al.*, 2011). Thus, we assayed mutant Na$_V$1.4-Y401C-N404R with 1 μM μ-CnIIIC and found that it had no effect on the remaining current and slightly slowed down the onset of block (I_{rem} = 7.8 ± 1.0%, τ_{on} = 308 ± 31 s, n = 6, Figure 3). Thus, the effect of the Na$_V$1.5 domain I pore loop must be accounted for by regions other than the inner pore residues C401 and R404.

Based on a first-order reaction scheme, an apparent IC_{50} of 1.3 nM and an almost vanishing off-rate of 4.6 10^{-6} s^{-1} was determined for wild-type rNa$_V$1.4 (Figure 1; Favreau *et al.*, 2012). Insertion of pore loops from Na$_V$1.5 not only altered the degree of block and its on-rate but also accelerated the off-rate, that is, made the toxin effect reversible (Figure 4A–C). Also, if the information on the kinetics of block relief upon toxin washout is taken into account, an apparent IC_{50} value and the kinetic constants can be estimated more accurately (Figure 4C): Ip5 – r_∞ = 5.1 ± 0.1%, k_{on} = 7.4 ± 0.1 10^3 $M^{-1}{\cdot}s^{-1}$, k_{off} = 5.3 ± 0.2 10^{-3} s^{-1}, IC_{50} = 708 ± 29 nM; IIp5 – r_∞ = 4.4 ± 0.1%, k_{on} = 243 ± 1 10^3 $M^{-1}{\cdot}s^{-1}$, k_{off} = 0.7 ± 0.1 $10^{-3}{\cdot}s^{-1}$, IC_{50} = 2.7 ± 0.5 nM. Thus, the pore loop in domain I has a strong effect on the equilibrium constant, while the pore loop in domain II does not change the IC_{50} but strongly affects the kinetics of toxin binding and dissociation. Na$_V$1.5 determinants do not increase the on-rate of μ-CnIIIC binding while leaving the channel largely unblocked, but the on-rate increase is accompanied by an even larger off-rate increase, resulting in lower overall affinity.

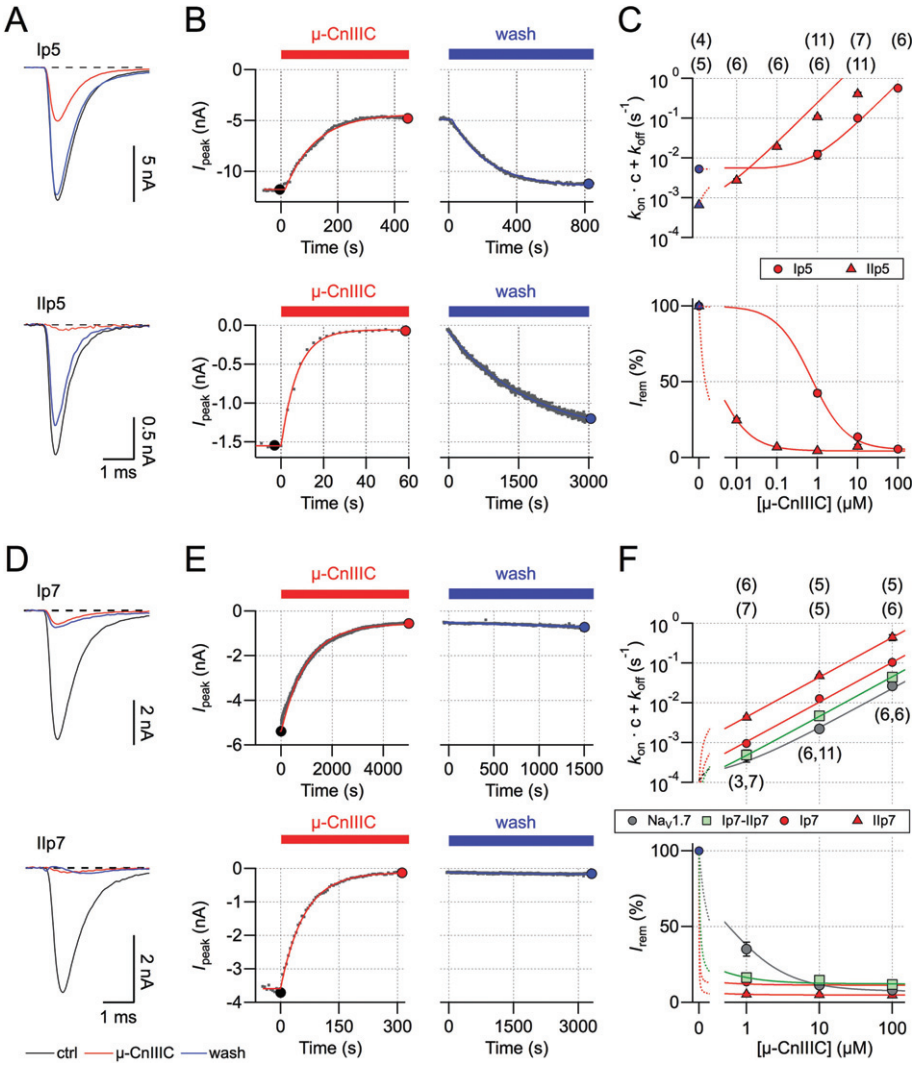

Figure 4

Analysis of pore-loop chimeras. (A) Superposition of current traces at −20 mV before (black) and after application of 1 μM μ-CnIIIC (red), as well as upon toxin washout (blue) for chimeras Ip5 (top) and IIp5 (bottom). (B) Time courses of toxin-induced current block and recovery kinetics upon wash with superimposed single-exponential fits. Solid symbols indicate data points from current traces shown in (A). (C) Kinetic analysis based on steady-state block and kinetics measured for various μ-CnIIIC concentrations. Lines are global data fits according to equations 1–2 for Ip5 (circles) and IIp5 (triangles). The *n* values are shown in parentheses. (D–F) Similar experiments as in (A–C) but for chimeras Ip7, IIp7 and Ip7-IIp7. The grey symbols in (F) indicate data for wild-type $hNa_V1.7$.

A similar experiment was performed for the pore loops of $Na_V1.7$. As shown in Figure 4D–F, neither of the pore loops inserted into $Na_V1.4$ made the toxin effect clearly reversible. Similar to the $Na_V1.5$ pore loops, toxin on-rate was faster for IIp7 than for Ip7, but neither of the pore loops substantially increased the IC_{50} value, which would reflect a $Na_V1.7$ phenotype. The combination of both pore loops resembled the properties of $Na_V1.7$ more closely. Based on the kinetics and steady-state block, the following parameters were estimated: $hNa_V1.7$ – r_∞ = 7.3 ± 0.9%, k_{on} = 0.23 ± 0.01 10^3 $M^{-1}{\cdot}s^{-1}$, k_{off} = 111 ± 21 $10^{-6}{\cdot}s^{-1}$, IC_{50} = 489 ± 94 nM; Ip7-IIp7 – r_∞ = 12.2 ± 0.4%, k_{on} = 0.45 ± 0.02 10^3 $M^{-1}{\cdot}s^{-1}$, k_{off} = 23 ± 3 $10^{-6}{\cdot}s^{-1}$, IC_{50} = 50.4 ± 6.6 nM; Ip7 – r_∞ = 11.4 ± 0.4%, k_{on} = 1.04 ± 0.05 10^3 $M^{-1}{\cdot}s^{-1}$, k_{off} = 9.1 ± 1.0 10^{-6} s^{-1}, IC_{50} = 8.7 ± 1.1 nM; IIp5 – r_∞ = 4.9 ± 0.1%, k_{on} = 4.4 ± 0.1 10^3 $M^{-1}{\cdot}s^{-1}$, k_{off} = 21 ± 7 10^{-6} s^{-1}, IC_{50} = 4.7 ± 1.8 nM.

Persistent but incomplete channel block

An interesting feature of μ-CnIIIC is its incomplete block, leaving a remaining current of about 5% for $Na_V1.4$ channels. To better understand this residual current component, we employed non-stationary noise analysis of current sweeps recorded in the whole-cell mode before and after toxin application. Simultaneous fit of ensemble variance versus mean current for three different voltages (–30, –10, 10 mV) under control conditions and upon saturation with 10 μM μ-CnIIIC (Figure 5A and B) yielded estimates for the maximal open

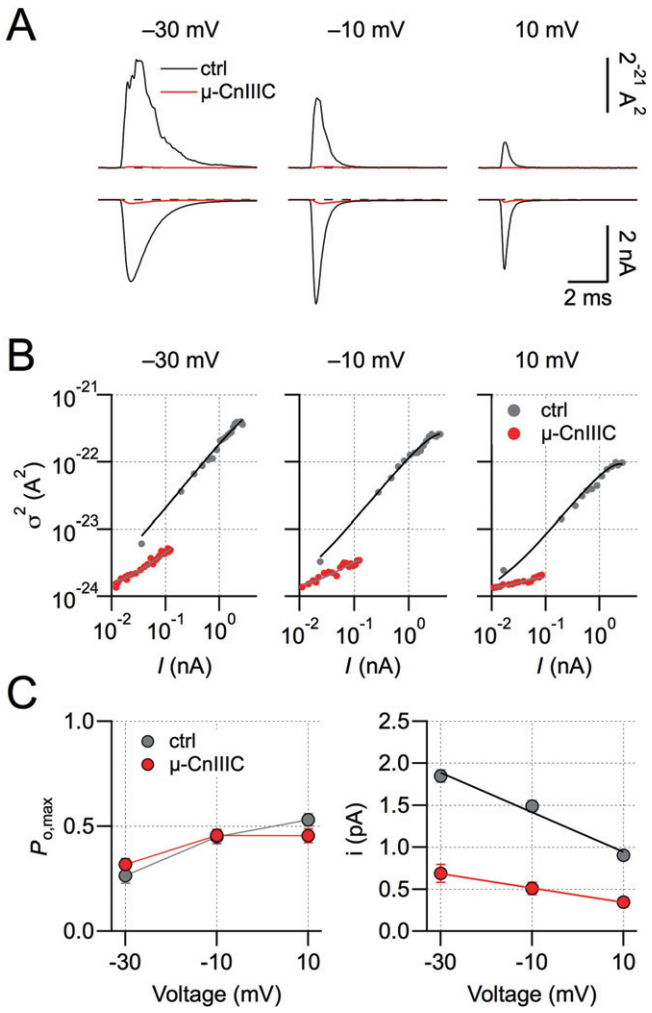

Figure 5

Single-channel characteristics. (A) Mean current and ensemble variance of rNa$_V$1.4 channels at the indicated voltages based on 200 individual current recordings before (black) and after application of 10 μM μ-CnIIIC (red). (B) Ensemble variance as a function of mean current for the indicated voltages without and with toxin. Continuous lines are fits according to equation 3. (C) Voltage-dependence of the maximal open probability and the single-channel current amplitude derived from non-stationary noise analysis. Lines connect the data points in the left panel; straight lines in the right panel are linear fits for determination of the chord conductance; n = 7.

probabilities and the single-channel current amplitude (Figure 5C). While $P_{o,max}$ did not change after toxin application (Figure 5C, left), the single-channel conductance was reduced from 23.6 ± 3.3 pS to 8.5 ± 2.9 pS (Figure 5C, right, n = 7). The total number of active channels was reduced to 14%. These results show that the residual current remaining in the presence of a saturating μ-CnIIIC concentration is carried by Na$_V$ channels with strongly reduced Na^+ conductance but without marked changes in the voltage-dependence of activation. The reduced number of active channels presumably reflects channels that are either blocked completely or that have entered some kind of hibernating state not accessible to non-stationary noise analysis.

Even if channel expression in HEK 293 cells is high, the current amplitude after μ-CnIIIC application is rather small and comparable to the current sizes sometimes observed in these cells that do not express exogenous Na$_V$ channels. Thus, to eliminate the possibility that the residual current results from the activity of μ-CnIIIC-insensitive endogenous channels, we performed experiments using the channel mutant rNa$_V$1.4-M1305C. Under control conditions, this mutant shares most of the kinetic properties of rNa$_V$1.4 wild-type channels (not shown), and it would not be expected to influence toxin sensitivity because the mutation is located in the intracellular domain III-IV linker (Figure 2A). When treated with 100 μM of the membrane-permeable cysteine-specific agent DTNP, rapid channel inactivation was removed almost completely (Figure 6A). Upon removal of DTNP, this non-inactivating current persisted and was subsequently blocked with 10 μM μ-CnIIIC, leaving a non-inactivating residual current of 4.2 ± 0.8%. This clearly shows that the residual μ-CnIIIC-resistant current is associated with mutant Na$_V$1.4-M1305C and not with any current component endogenous to HEK 293 cells (Figure 6A and C).

With this unambiguous identification of the tiny current remaining after μ-CnIIIC application, we determined whether the pore blocker TTX has an effect on this current. Rapid inactivation of Na$_V$1.4-M1305C channels was first removed by applying DTNP. The resulting non-inactivating channels were readily blocked with 1 μM TTX (95.4 ± 0.5%; Figure 6B and C, n = 6). However, TTX only had a small effect on the residual current leaking through μ-CnIIIC-occupied channels (11.6 ± 3.0% blockade; Figure 6A and C, n = 6). This result strongly suggests that Na$_V$1.4 channels, once occupied by μ-CnIIIC, are not readily accessible to TTX, that is, TTX cannot reach its binding site in the channel pore. When μ-CnIIIC (1 μM) and TTX (100 μM) were co-applied, the channels were blocked rapidly such as with TTX alone (Figure 6D). However, upon washing with control saline, slow recovery was observed; whereas when TTX was applied alone the block was rapidly removed and with μ-CnIIIC alone no recovery occurred. This experiment suggests that μ-CnIIIC can block the channel with TTX being located at receptor site-1.

Discussion and conclusions

μ-CnIIIC is a promising candidate for further clinical development

The μ-conopeptide CnIIIC shows selectivity across Na$_V$ subtypes in rodents, displaying strong activity against rat skeletal muscle Na$_V$1.4 and rat brain Na$_V$1.2 channels while being inactive with respect to cardiac mouse Na$_V$1.5 and rat Na$_V$1.8 channels (Favreau *et al.*, 2012). Previous work on a pair of different μ-conotoxins, μ-GIIIA and μ-GIIIB, indicated that channel selectivity observed in rodents is not necessarily observed in humans (Cummins *et al.*, 2002). However, in the case of μ-CnIIIC, we have shown in this study that the selectivity observed for the rodent channels is fully reproduced in their human paralogs. These similarities in potency and selectivity of rodent and human channels, together with efficacy seen *in vivo* experiments (Favreau *et al.*, 2012), strongly

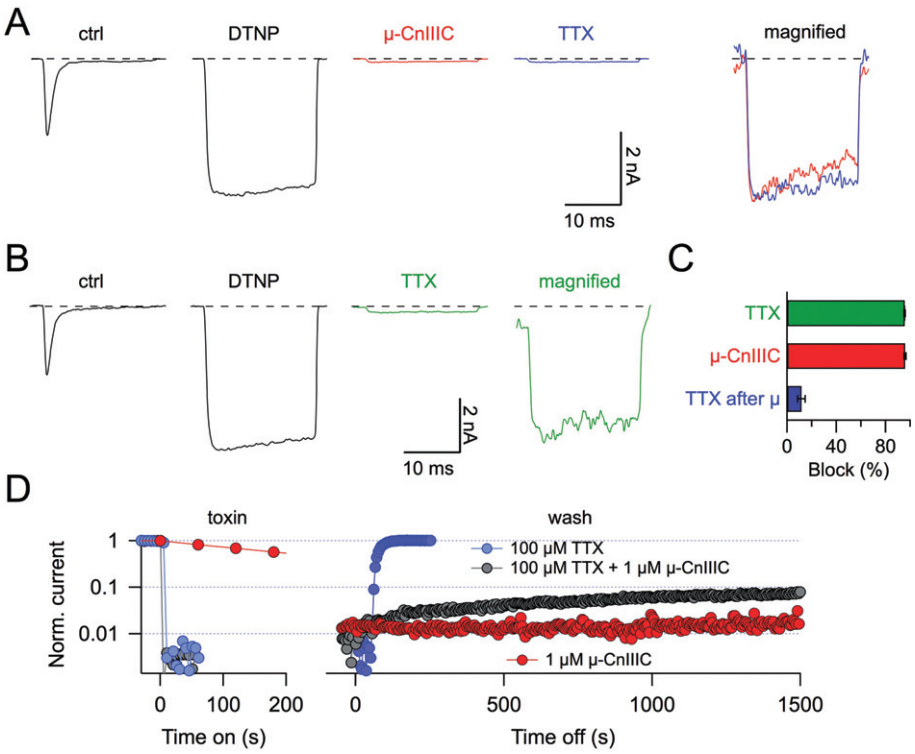

Figure 6

TTX block of non-inactivating, μ-CnIIIC-occupied channels. (A) Current responses at −20 mV of a HEK 293 cell expressing rNa$_V$1.4-M1305C channels, under control conditions (ctrl), after application of 100 μM DTNP (DTNP), after subsequent application of 10 μM μ-CnIIIC without DTNP and finally after application of 1 μM TTX without DTNP or μ-CnIIIC. The panel on the right shows a magnified superposition of DTNP-modified traces with μ-CnIIIC (red) and subsequent TTX application (blue). (B) Similar experiment as in (A) but without application of μ-CnIIIC illustrating that 1 μM TTX potently blocks DTNP-modified channels. (C) Statistics of current block of non-inactivating rNa$_V$1.4-M1305C channels induced by 1 μM TTX, 10 μM μ-CnIIIC or 1 μM TTX after equilibration in 10 μM μ-CnIIIC ($n = 6$), illustrating that the current remaining after μ-CnIIIC block is not readily sensitive to TTX. (D) Block kinetics and recovery kinetics of DNTP-modified rNa$_V$1.4-M1305C channels after the application of 100 μM TTX, the same concentration of TTX together with 1 μM μ-CnIIIC or 1 μM μ-CnIIIC alone.

support the further clinical development of μ-CnIIIC. With an apparent IC$_{50}$ value of a few nM for Na$_V$1.4, there is a safety margin towards cardiac Na$_V$1.5 of more than 1000-fold, thus reducing the risk of cardiac side effects to a very low level. An important feature of μ-CnIIIC is its very long-lasting block with estimated reversibility time constants in the order of many hours. This stability was not compromised in solutions of varying pH (supporting information Figure S1), thus explaining the long-lasting effects also seen in an *in vivo* setting.

Dissection of molecular determinants of μ-CnIIIC selectivity

A detailed understanding of how μ-conotoxins interact with and block Na$_V$ channel subtypes is therefore likely to be the key to future drug development. Using chimeras between μ-CnIIIC-sensitive (Na$_V$1.4) and insensitive channel subtypes (Na$_V$1.5 and Na$_V$1.8), we attempted to localize molecular determinants for the toxin insensitivity. While replacing domains of Na$_V$1.4 with corresponding structures from either the first and or the second half of Na$_V$1.8 was sufficient to eliminate toxin sensitivity, substituting domains from the second half of Na$_V$1.5 into Na$_V$1.4 had no detectable effect. Thus, in Na$_V$1.8, all four domains harbour sites that are incompatible with μ-conotoxin activity, while for Na$_V$1.5, the determinants are located exclusively in domains I and II. At a higher resolution, our investigation revealed that the structural determinants for μ-CnIIIC insensitivity are located in the pore loops of these domains. However, the pore loops in domains I and II contribute to toxin insensitivity in different ways. While the pore loop of domain I strongly increased the apparent IC$_{50}$ of μ-CnIIIC, the pore loop of domain II had little effect on steady-state toxin binding but accelerated toxin association and dissociation. One interpretation of this observation with respect to Na$_V$1.4 would be that while domain I is key to high-affinity toxin binding, domain II affects access of the toxin to its binding site. However, the effect of domain I pore loop is not mediated by those residues determining the different TTX sensitivity of Na$_V$1.4 and Na$_V$1.5 channels, suggesting that other parts of the pore loop must play an important role.

Apparently, the effect of different channel fragments on the μ-conotoxin block strongly depends on the conotoxin investigated. For example, for μ-SIIIA, a related toxin with only a few structural differences compared with μ-CnIIIC (Leipold *et al.*, 2011), the influence of the domain I pore loop on channel block was attributable to the TTX site, but the

major functional difference between $Na_V1.4$ and $Na_V1.5$ channels was mediated by the pore loop in domain II. In contrast, the TTX site does not have a functional effect on μ-CnIIIC activity, although the domain I pore loop determines the sensitivity of the channel to μ-CnIIIC.

Moreover, the μ-SIIIA phenotypes of $rNa_V1.4$ and $hNa_V1.7$ could be bidirectionally conferred by the substitution of only a single residue in the domain II pore loops of these channels ($rNa_V1.4$: A728, $hNa_V1.7$: N889, supporting information Figure S2). In contrast, even the exchange of the entire pore loop II was not sufficient to confer the μ-CnIIIC phenotype of $Na_V1.7$ to $Na_V1.4$ (Figure 4). Similar to $Na_V1.5$, pore loop I of $Na_V1.7$ appeared to play an important role in determining the activity of the toxin. Given the weak sequence conservation of that pore loop among the various Na_V channel isoforms (supporting information Figure S2B), it will be a huge challenge to design a toxin specific for $Na_V1.7$, for example, as an analgesic.

Residual current upon saturation with μ-CnIIIC

An interesting feature of certain μ-conotoxins is that they apparently do not achieve complete blockade of sodium channels. Using a variant of μ-GIIIA (R13Q) that leaves about 25% of the rat $Na_V1.4$ current unblocked, French *et al*. (1996) studied the properties of μ-conotoxin-occupied channels, showing that the bound toxin both reduces the single-channel current size and slightly modifies channel gating. Subsequently, it was demonstrated that TTX can enter the pore to reach toxin receptor site-1 when the channel is bound by μ-GIIIA (R13Q) (Zhang *et al*., 2010). Here, we showed that μ-CnIIIC, similar to μ-SIIIA (Leipold *et al*., 2011), is an example of a natural μ-conotoxin that fails to block $Na_V1.4$ channels completely, albeit with a residual current of only about 5% of the total control amplitude. This illustrates that the phenomenon of 'leaky channel block' is not a feature restricted to μ-conotoxin mutants but is also observable for native toxins. However, owing to the small amplitude of the remaining current fraction, such current signals are not accessible to direct single-channel recordings. We thus used non-stationary noise analysis to show that the remaining current was mediated by a fraction of μ-CnIIIC-occupied channels with reduced single-channel conductance; apparently, another fraction of channels was either completely blocked or went into another non-conducting state.

Unambiguous assignment of 5% residual current to exogenously expressed channels was demonstrated using a channel mutant, which had a fast inactivation that was removed by the extracellular application of DTNP. In addition, using this method, it was shown that the current remaining after saturation with μ-CnIIIC is not readily accessible to TTX block. Thus, we conclude that μ-CnIIIC blocks access of TTX to channel receptor site-1. Likewise, other low molecular weight drugs accessing receptor site-1 might not be active on μ-CnIIIC-occupied channels. On the other hand, once TTX is bound to the channel, μ-CnIIIC is apparently still able to bind to its receptor site, as demonstrated by an accelerated recovery from μ-CnIIIC block in the presence of TTX. Thus, the channel's extracellular cavity must be wide enough to simultaneously accommodate TTX and the μ-conopeptide CnIIIC, similar to μ-KIIIA (Zhang *et al*., 2010). The incomplete recovery of μ-CnIIIC block in the presence of TTX (Figure 6D) and the results from non-stationary noise analysis are suggestive of more than a single configuration by which the toxin can occupy the channel's pore.

Conclusions

The μ-conopetide CnIIIC from *Conus consors* is a very potent, selective and durable antagonist of skeletal muscle $Na_V1.4$ sodium channels (Favreau *et al*., 2012). In this study, we have shown that this promising pharmacological profile is fully reproduced in the relevant human sodium channels, providing important confirmation of the clinical potential of μ-CnIIIC as a muscle relaxant. Further development may benefit from a better understanding of the molecular basis underlying the channel selectivity of μ-CnIIIC, and in this study, we showed that the structural basis for selectivity against $Na_V1.8$ is relatively complex, involving structures located in channel domains III and IV in addition to domains I and II. By contrast, determinants of selectivity for $Na_V1.5$ and $Na_V1.7$ reside in the pore loops of domains I and II. Future attempts to optimize the effects of μ-CnIIIC for potential clinical applications, by increasing its safety margin with respect to cardiac $Na_V1.5$ or by improving its pharmacokinetic properties, should therefore focus on the interaction of this toxin with the pore loop elements of the first two channel domains.

Acknowledgements

This work was supported by the European Union FP6 (CONCO). We thank JS Trimmer for providing cDNA coding for $rNa_V1.4$, Ch. Alzheimer for $hNa_V1.2$, AL George for $hNa_V1.4$, $hNa_V1.5$, N Klugbauer for $hNa_V1.7$ and JN Wood for $rNa_V1.8$.

Conflicts of interest

None to declare.

References

Alexander SPH, Mathie A, Peters JA (2011). Guide to Receptors and Channels (GRAC), 5th edition. Br J Pharmacol 164 (Suppl. 1): S1–S324.

Andavan GS, Lemmens-Gruber R (2011). Voltage-gated sodium channels: mutations, channelopathies and targets. Curr Med Chem 18: 377–397.

Backx PH, Yue DT, Lawrence JH, Marban E, Tomaselli GF (1992). Molecular localization of an ion-binding site within the pore of mammalian sodium channels. Science 257: 248–251.

Chahine M, Sirois J, Marcotte P, Chen L, Kallen RG (1998). Extrapore residues of the S5–S6 loop of domain 2 of the voltage-gated skeletal muscle sodium channel (rSkM1) contribute to the μ-conotoxin GIIIA binding site. Biophys J 75: 236–246.

Chen H, Gordon D, Heinemann SH (2000). Modulation of cloned skeletal muscle sodium channels by the scorpion toxins Lqh II, Lqh III, and Lqh αIT. Pflügers Arch 439: 423–432.

Choudhary G, Yotsu-Yamashita M, Shang L, Yasumoto T, Dudley SC Jr (2003). Interactions of the C-11 hydroxyl of tetrodotoxin with the sodium channel outer vestibule. Biophys J 84: 287–294.

Cummins TR, Aglieco F, Dib-Hajj SD (2002). Critical molecular determinants of voltage-gated sodium channel sensitivity to μ-conotoxins GIIIA/B. Mol Pharmacol 61: 1192–1201.

Dudley SC Jr, Todt H, Lipkind G, Fozzard HA (1995). A μ-conotoxin-insensitive Na^+ channel mutant: possible localization of a binding site at the outer vestibule. Biophys J 69: 1657–1665.

Dudley SC Jr, Chang N, Hall J, Lipkind G, Fozzard HA, French RJ (2000). μ-conotoxin GIIIA interactions with the voltage-gated Na^+ channel predict a clockwise arrangement of the domains. J Gen Physiol 116: 679–690.

Favreau PH, Benoit E, Hocking H, Carlier L, D'hoedt D, Leipold E *et al*. (2012). Pharmacological characterization of a novel μ-conopeptide, CnIIIC, indicates potent and preferential inhibition of sodium channel subtypes ($Na_V1.2/1.4$) and reveals unusual activity on neuronal nicotinic acetylcholine receptors. Br J Pharmacol 166: 1654–1668.

French RJ, Prusak-Sochaczewski E, Zamponi GW, Becker S, Kularatna AS, Horn R (1996). Interactions between a pore-blocking peptide and the voltage sensor of the sodium channel: an electrostatic approach to channel geometry. Neuron 16: 407–413.

George AL Jr (2005). Inherited disorders of voltage-gated sodium channels. J Clin Invest 115: 1990–1999.

Goldin AL (2002). Evolution of voltage-gated Na^+ channels. J Exp Biol 205: 575–584.

Heinemann SH, Leipold E (2011). Tools for studying peptide toxin modulation of voltage-gated sodium channels. In e-book: Toxins and Ion Transfers, SFET Editions. http://www.sfet.asso.fr.

Heinemann SH, Terlau H, Imoto K (1992). Molecular basis for pharmacological differences between brain and cardiac sodium channels. Pflügers Arch 422: 90–92.

Jurman ME, Boland LM, Liu Y, Yellen G (1994). Visual identification of individual transfected cells for electrophysiology using antibody-coated beads. Biotechniques 17: 876–881.

Leipold E, Markgraf R, Miloslavina A, Kijas M, Schirmeyer J, Imhof D *et al*. (2011). Molecular determinants of the subtype specificity of μ-conotoxin SIIIA targeting neuronal voltage-gated sodium channels. Neuropharmacology 61: 105–111.

Li RA, Ennis IL, French RJ, Dudley SC Jr, Tomaselli GF, Marban E (2001). Clockwise domain arrangement of the sodium channel revealed by μ-conotoxin (GIIIA) docking orientation. J Biol Chem 276: 11072–11077.

Norton RS (2010). Mu-conotoxins as leads in the development of new analgesics. Molecules 15: 2825–2844.

Priest BT (2009). Future potential and status of selective sodium channel blockers for the treatment of pain. Curr Opin Drug Discov Devel 12: 682–692.

Schirmeyer J, Szafranski K, Leipold E, Mawrin C, Platzer M, Heinemann SH (2010). A subtle alternative splicing event of the $Na_V1.8$ voltage-gated sodium channel is conserved in human, rat, and mouse. J Mol Neurosci 41: 310–314.

Sigworth FJ (1977). Sodium channels in nerve apparently have two conductance states. Nature 270: 265–267.

Starkus JG, Varga Z, Schönherr R, Heinemann SH (2003). Mechanisms of the inhibition of Shaker potassium channels by protons. Pflügers Arch 447: 44–54.

Wood JN, Boorman JP, Okuse K, Baker MD (2004). Voltage-gated sodium channels and pain pathways. J Neurobiol 61: 55–71.

Zhang MM, Gruszczynski P, Walewska A, Bulaj G, Olivera BM, Yoshikami D (2010). Cooccupancy of the outer vestibule of voltage-gated sodium channels by μ-conotoxin KIIIA and saxitoxin or tetrodotoxin. J Neurophysiol 104: 88–97.

Zuliani V, Rivara M, Fantini M, Costantino G (2010). Sodium channel blockers for neuropathic pain. Expert Opin Ther Pat 20: 755–779.

Supporting information

Additional Supporting Information may be found in the online version of this article:

Figure S1 Block of $rNa_V1.4$ channels at various pH values. (A) Current traces of $rNa_V1.4$ channels at –20 mV before and after application of 10 μM μ-CnIIIC, as well as upon wash with control saline (pH 7.4), followed by wash with solution of pH 6.5 and pH 8.0. In the panel on the right all traces are superimposed, scaled to peak. (B) Time course of peak inward current for the indicated conditions. (C) Statistics on recovery from μ-CnIIIC block for 200-s wash each, obtained with solutions of the indicated pH values. *n*-values are provided in parentheses.

Figure S2 Sequence alignments of Na_V-channel regions particularly important for μ-conotoxin action. (A) Topological cartoon of an Na_V α-subunit with four homologous domains (DI-DIV). Boundaries used for the construction of domain chimeras (red diamonds) and pore loop chimeras (colour) are indicated. Residue numbers refer to $rNa_V1.4$. (B) Multiple sequence alignments of the indicated Na_V-channel types for the pore region of domain I (pink) and of domain II (blue).

Please note: Wiley-Blackwell are not responsible for the content or functionality of any supporting materials supplied by the authors. Any queries (other than missing material) should be directed to the corresponding author for the article.